Research Square

Preprints are preliminary reports that have not undergone peer review.
They should not be considered conclusive, used to inform clinical practice,
or referenced by the media as validated information.

Isolating the texture effect on corrosion property of ultra-fine-grained high-purity magnesium

Junsong Zheng
Nanjing University of Science & Technology
Kainning Wang
Nanjing University of Science & Technology
Jingtao Wang
Nanjing University of Science & Technology
Zheng Li
lizheng@njust.edu.cn

Nanjing University of Science & Technology

Article

Keywords: Severe plastic deformation, immersion testing, electrochemistry, dislocation density, texture intensity

Posted Date: November 2nd, 2026

DOI: https://doi.org/10.21203/rs.3.rs-11334735/v1

License: This work is licensed under a Creative Commons Attribution 4.0 International License.
Read Full License

Additional Declarations: No competing interests reported.

Isolating the texture effect on corrosion property of ultra-fine-grained high-purity magnesium

Abstract

Magnesium is considered a promising biodegradable biomedical material, but its overly fast corrosion and degradation have become a key limitation for clinical applications. In this study, by controlling the grain size of high-purity magnesium while keeping the texture intensity almost unchanged, we only looked at how dislocation density affects its corrosion rate. We found that as the dislocation density increases, the sample's corrosion rate keeps speeding up, and the acceleration frequency also rises. Additionally, by keeping the grain size constant through processing methods, we explored how dislocation density and strong basal texture affect the corrosion rate of high-purity magnesium. Combining the isolated effect of dislocation density obtained in this work, we could isolate dislocation density and just examine how strong basal texture impacts the corrosion performance of high-purity magnesium. The results show that as texture intensity increases, high-purity magnesium's corrosion resistance also improves. This is because the basal plane has the best corrosion resistance, and as the texture intensity rises, the proportion of basal plane increases, leading to a decrease in the corrosion rate in m-SBF. Eventually, we established a phenomenological model relating texture intensity to the corrosion rate of high-purity magnesium.

Keywords: Severe plastic deformation; immersion testing; electrochemistry; dislocation density; texture intensity

1. Introduction

In recent years, magnesium-based materials have attracted a lot of attention as third-generation biomedical materials for use as clinically degradable implants because they are fully degradable, have good biocompatibility, antibacterial properties, and excellent human compatibility[1][2]. Currently, various magnesium-centered degradable implants, such as bone screws, in vivo stents, and vascular clips[3], have entered clinical trials. However, the overly rapid degradation of magnesium-based implants in the body can seriously affect their mechanical performance and biocompatibility[4], which remains a key bottleneck limiting their clinical application. Due to breakthroughs in alloy technology, most researchers nowadays focus on improving the properties of magnesium alloys and exploring surface modification techniques, while research on high-purity magnesium, especially the performance breakthroughs of high-purity magnesium (99.99 wt%), is still rare[5].To address the fast corrosion rate of high-purity magnesium, researchers have extensively studied factors affecting magnesium corrosion, including grain size[6], dislocations[7], and grain orientation[8]-[10].By controlling microstructures like grain size, dislocation density, and texture, it's possible to adjust corrosion behavior without changing the chemical composition. So, studying the relationship between the microstructure of high-purity magnesium and its corrosion performance is really important for understanding bio-corrosion mechanisms and accurately controlling the degradation rate.

Many studies have shown that under fine-grain conditions, as grain size decreases, the corrosion rate of high-purity magnesium decreases, which is attributed to the formation of a more uniform and coherent passivation layer due to grain refinement, with more grain boundaries acting as barriers to preferential crystal pitting[11][12]. Additionally, dislocation density is thought to be positively correlated with the corrosion rate of high-purity magnesium, meaning that higher dislocation density leads to faster corrosion, but studies specifically regulating dislocation density to explore its effect on high-purity magnesium corrosion *are few*. Regarding texture research, many scholars focus on how different crystal plane textures affect corrosion rates[13][14], often *ignoring* the effect of single texture intensity on corrosion rates.

In practice, during sample preparation, grain size and dislocation density change along with texture intensity, making it difficult to separate the effects of the two and, therefore, hard to isolate a quantitative relationship between corrosion performance and texture intensity. In this study, we used a t-HPS severe plastic deformation technique independently developed by our research group to prepare fine-grained high-purity magnesium. This technique allows the grain size to refine to an ultrafine level, and with increasing t-HPS turns, the grain size hardly changes, which helps eliminate the effect of grain size. Then, by applying varying degrees of compressive strain at room temperature, we found that the fine-grained high-purity magnesium samples showed changes in dislocation density while the grain size and texture intensity barely changed. This controlled a single variable, allowing us to study only the effect of dislocation density on high-purity magnesium samples. Using electrochemical and immersion tests, we investigated the corrosion behavior of these fine-grained high-purity magnesium samples, directly revealing the relationship between dislocation density and the corrosion rate of high-purity magnesium. By combining compression with t-HPS, we can obtain samples with changes in texture intensity only, enabling us to focus solely on

how texture intensity affects the corrosion rate of high-purity magnesium. These studies are significant for future researchers who want to delve deeper into how the microstructure of high-purity magnesium affects its corrosion rate.

2. Experimental Methods

2.1. Processing Methods

The materials used in this experiment were high-purity magnesium (99.99 wt%). The original samples were cast samples, which were machined into tubular split-tip specimens with a height of 11 mm, an inner diameter of 22.5 mm, a semi-conical angle of 10°, and a wall thickness of 2 mm. The samples were first stress-relief annealed at 300°C for 6 hours, then polished on the surface. After that, the samples were subjected to severe plastic deformation using the t-HPS (tube high-pressure shearing) method[15]. The cut size of the samples after t-HPS was 9×10×2 mm. For the first group, the samples were first treated with 20 turns of t-HPS at 100°C, then the cut samples were compressed to four different levels: 10%, 15%, 20%, and 25%, with a compression error within 2%. This group was called the compression strain group. The second group of samples was treated with t-HPS for 10, 15, 20, and 25 turns at 150°C to study texture intensity as required by the experiment. This group was called the different turns group, and three parallel samples were obtained for each treatment.

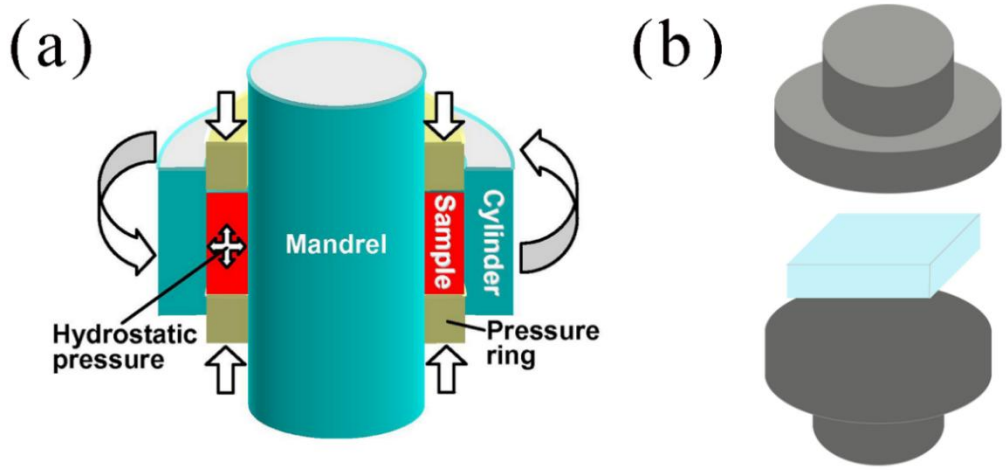


Figure 1 Processing diagram: (a) t-HPS diagram[16];(b) Compression diagram

2.2. Microscopic Structure Analysis

EBSD analysis was done using the Zeiss CrossBeam 350 to study the microstructural features of the material, including grain size, dislocation density, grain orientation, and texture intensity. The sample surfaces was electro-polished with commercial AC_2 solution for 52 seconds at 10°C after basic grinding and diamond polishing down to a surface roughness of 0.5μm. The EBSD results were processed with Channel 5 analysis software. To examine the corrosion morphology of high-purity magnesium samples, a GeminiSEM 360 scanning electron microscope was used, and energy-dispersive spectroscopy (EDS) was applied to analyze the corrosion products.

2.3. Corrosion Performance Test

2.3.1. Electrochemical corrosion test

Electrochemical corrosion tests were carried out in modified simulated body fluid (m-SBF) with a pH of 7.4. A three-electrode system was used for the tests, where the sample, platinum electrode, and saturated calomel electrode (SCE) acted as the working, counter, and reference electrodes, respectively. The exposed area of the sample was 0.2826 cm^2. After the open circuit potential (OCP) stabilized for 1 hour, electrochemical impedance spectroscopy (EIS) measurements were taken over a frequency range of 100 kHz to 0.01 Hz with a perturbation amplitude of 5 mV. For potentiodynamic polarization tests, potentials ranging from OCP -500 mV to 500 mV were applied at a scan rate of 2 mV/s.

2.3.2. Immersion Test

The immersion test used a constant temperature water bath to submerge the samples in m-SBF solution at 37.5±0.5°C for 168 hours. To simulate the real human environment, the m-SBF solution was replaced every 24 hours. The ratio of m-SBF solution to the surface area of the sample was 20 ml/cm^2[17]. Before weighing, the

corroded samples were cleaned with a solution made of 200 g CrO_3, 10 g $AgNO_3$, and 1 L H_2O[18]. The corrosion rate of the samples was calculated using the following formula[17]:

$$CR= 8.76*10^4W/(A\ T\ D) \quad (1)$$

where W is the mass loss (g), A is the original surface area of each sample (cm^2), T is the immersion time (h), and D is the sample density (g/cm^3).

3. Experimental results

3.1. Test results of compression strain group

3.1.1. Microstructure testing of different compression strain groups

The microstructure of samples under different compressive strains can be seen in **Figure 2** (0% strain (Figure (a1)), 10% strain (Figure (b1)), 15% strain (Figure (c1)), 20% strain (Figure (d1)), 25% strain (Figure (e1))).

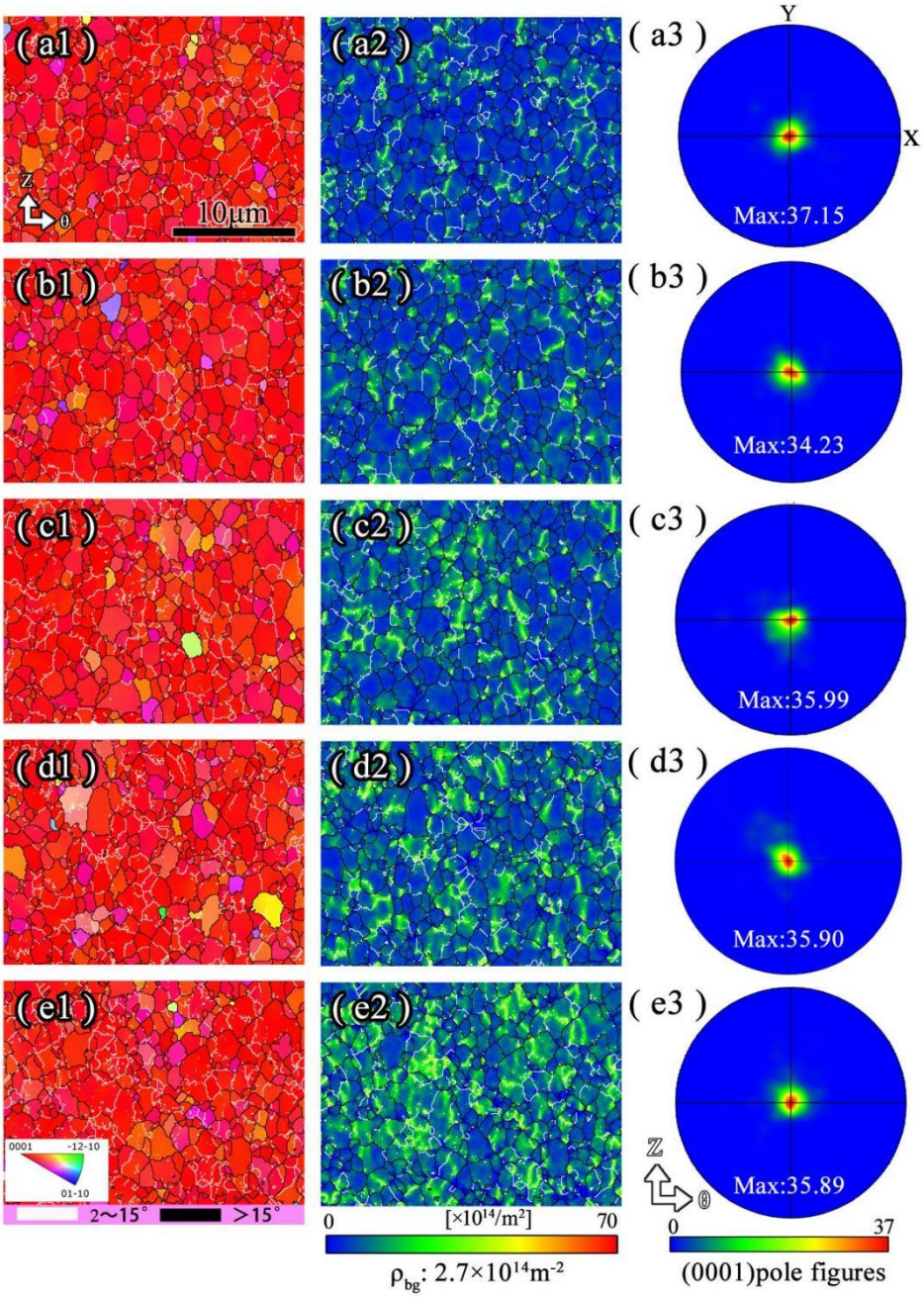


Figure 2 EBSD maps at different compressive strains: 0% Strain,10% Strain,15% Strain,20% Strain,25% Strain; microstructure images (a1～e1);geometrically necessary dislocation maps (a2～e2);(0001) pole figures (a3～e3)

From **Figure 2** (a1) to (e1), we can see that the texture of the samples is roughly consistent, and the grain sizes are very similar. A detailed analysis is shown in **Figure 3**. The average grain size ranges from *1.26 to 1.32*μm, which, within the margin of error, suggests that the grain size doesn't change during compression. Therefore, we can rule out the influence of grain size on the corrosion performance in this set of samples.

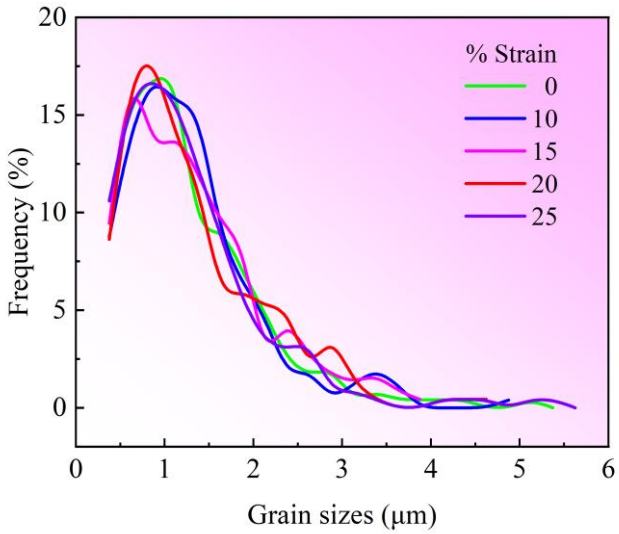


Figure 3 Grain size distribution chart of 20Turn 100℃ t-HPS under different compressive strains

The textures of these five samples, as shown in **Figure 2** (a3)～(e3), are very similar, with grains mainly oriented along (0001). The maximum texture intensitys at 0% to 25% compressive strain are 37.15,34.23,35.99, 35.90,and 35.89, respectively. This indicates that the texture intensity of this set of five samples has negligible impact on corrosion performance, so we can just consider the effect of dislocation density on the corrosion behavior of high-purity magnesium in m-SBF. From **Figure 2** (a2)～(e2), it can be seen that as the compressive strain increases, the dislocation density keeps increasing, being $6.67\pm0.18\times10^{14}/m^2$,$8.24\pm0.13\times10^{14}/m^2$,$9.26\pm0.21\times10^{14}/m^2$,$10.21\pm0.19\times10^{14}/m^2$,and $11.91\pm0.16\times10^{14}/m^2$ respectively.

3.1.2. Corrosion Tests for Different Compression Strain Groups

This study conducted a 168-hour m-SBF immersion test. **Figure 4** shows the mass loss of the samples after being immersed in m-SBF at 37±0.5°C for 168 hours. Among them, the uncompressed samples had a corrosion rate of 0.6572±0.0258mm/year,As can be seen from Figure 4, as the compressive strain increases, the dislocation density keeps rising, and the corrosion rate gets faster.

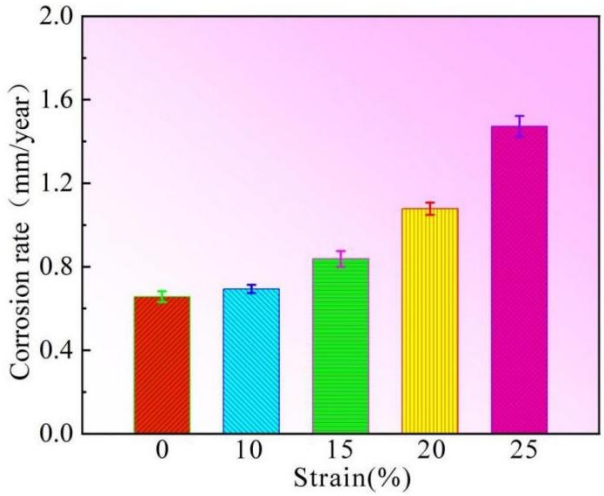


Figure 4 Schematic diagram of mass loss of high-purity magnesium samples under different compressive strains after 168h immersion test

To investigate the corrosion behavior of high-purity magnesium in SBF, SEM tests were carried out on samples soaked for 168 hours, and the results are shown in **Figure 5**. After immersion corrosion, a dense layer of corrosion products formed on the surface. Due to the internal stress generated during the dehydration of this dense layer, many cracks appeared on the surface. EDS results (see supplementary material 1) showed that all five sample groups contained Mg, O, Ca, and P elements. Oxygen was widely distributed, indicating the formation of a $Mg(OH)_2$/MgO corrosion layer on the surface, while Ca and P appeared together, suggesting that Ca^{2+} and PO_4^{3-} from the SBF further deposited on the corrosion products to form a Ca-P mineralized layer.

The specific corrosion process equations are as follows[19]:

$$HPO_4^{2-}+OH^- \rightarrow PO_4^{3-}+H_2O \quad (2)$$

$$3Ca^{2+}+2PO_4^{3-} \rightarrow Ca_3(PO_4)_2 \quad (3)$$

$$3Mg^{2+}+2PO_4^{3-} \rightarrow Mg_3(PO_4)_2 \quad (4)$$

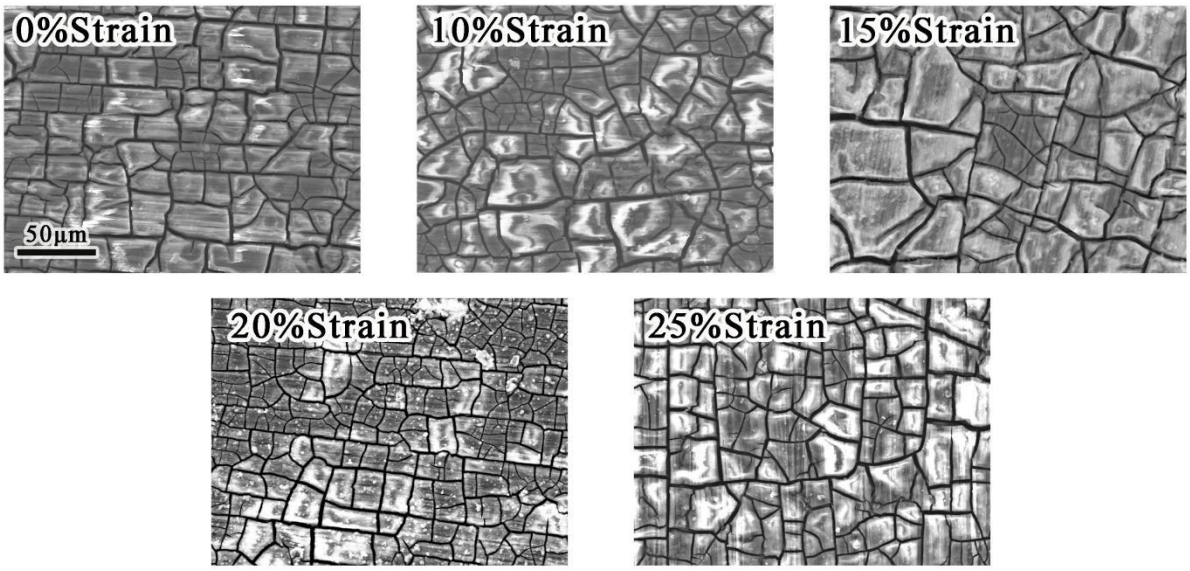


Figure 5 SEM schematic results of high-purity magnesium samples with different compressive strains after 168h immersion in SBF

Figure 6 shows the morphology after cleaning the corrosion products. From the figure, it can be seen that as the compressive strain increases, the corrosion pits clearly continue to increase, and the corrosion depth keeps getting deeper. At 25% strain, a large number of corrosion pits and some deep pitting are observed.

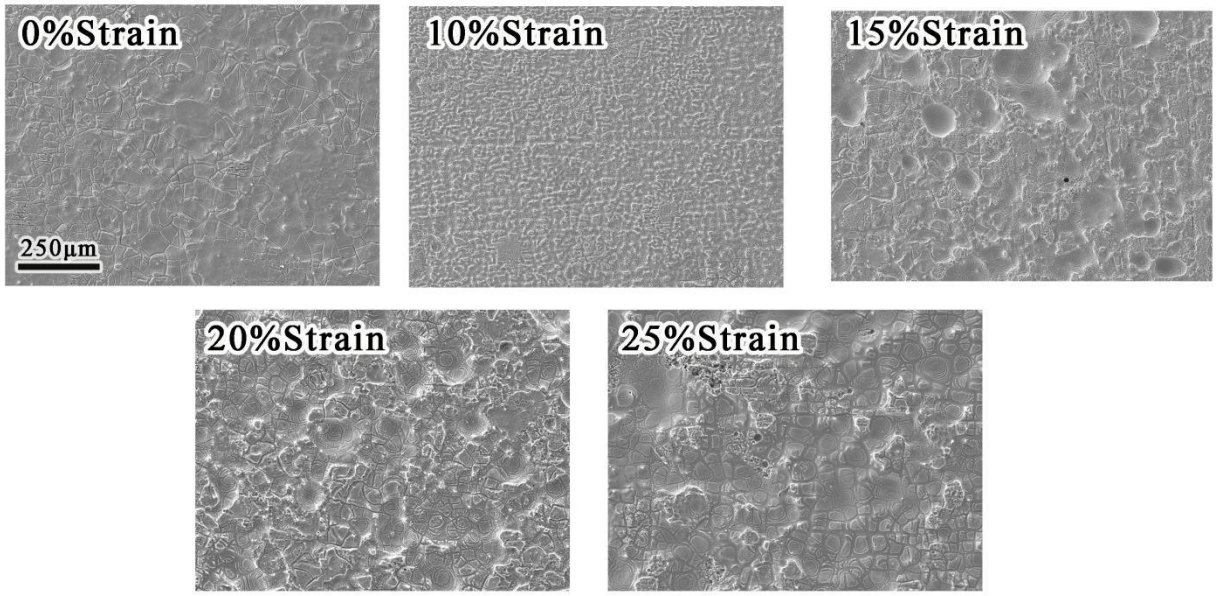


Figure 6 Schematic of SEM results after cleaning 168h SBF immersion test of high-purity magnesium samples with different compressive strains

The corrosion resistance of these samples was evaluated through electrochemical polarization curves, AC impedance spectra, and immersion tests in 37°C m-SBF solution, to understand how differences in dislocation density affect the corrosion rate. **Figure 7** shows the electrochemical polarization curves of the high-purity magnesium samples.

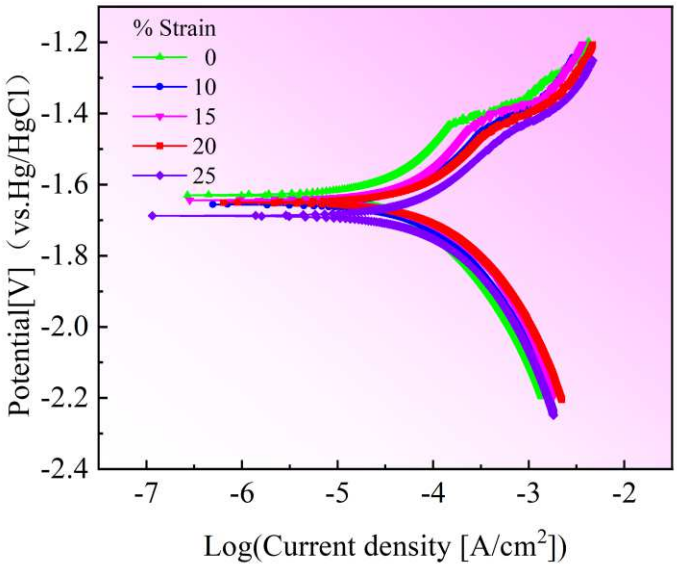


Figure 7 Electrochemical polarization curves of high-purity magnesium in m-SBF solution under different compressive strains

In these polarization curves, the cathodic side is controlled by the hydrogen evolution reaction in the aqueous solution, while the other side is the anodic oxidation reaction (that is, magnesium dissolution) and abnormal anodic hydrogen evolution, known as the negative difference effect [20]; obviously, the cathodic behavior of the five samples in this set of experiments is similar. The corrosion current density for the five samples is $2.20\times10^{-5}A/cm^2$、$3.68\times10^{-5}A/cm^2$、$3.75\times10^{-5}A/cm^2$、$4.61\times10^{-5}A/cm^2$、$4.64\times10^{-5}A/cm^2$.

This result shows that as the dislocation density increases, the corrosion rate of high-purity magnesium in m-SBF gradually speeds up. The corrosion potential (E) and corrosion current density (I) derived from these curves are listed in **Table 1**

Table 1 Corrosion voltage and corrosion current values of samples with different compressive strains in m-SBF solution

Strain（%）	Ecorr（V vs.Hg/HgCl）	Icorr（A/cm^2）
0	-1.63±0.04	2.20±0.12×10^{-5}
10	-1.65±0.02	3.68±0.16×10^{-5}
15	-1.64±0.05	3.75±0.12×10^{-5}
20	-1.65±0.06	4.61±0.15×10^{-5}
25	-1.69±0.03	4.64±0.14×10^{-5}

Figure 8 shows the EIS spectra of these samples after soaking in m-SBF solution for 1 hour.The Nyquist plots of the five samples show similar electrochemical behavior: they all have a large high-frequency capacitive loop, a mid-frequency capacitive loop, and a low-frequency inductive loop [21]. The large capacitive loop is caused by the corrosion product film formed on the surface [22], while the small capacitive loop is due to the charge transfer process in the double layer formed by Mg^{2+} on the surface film [23]. The inductive loop at low frequency is attributed to the relaxation process of adsorbed intermediates [24]. From the Bode plot of |Z| versus frequency in Figure 8(b), it's clear that the impedance of all samples increases from high to mid-low frequencies and then decreases at low frequencies, indicating the presence of an inductive loop at low frequency. The Bode plot of phase versus frequency shows two peaks, indicating the presence of two capacitive loops. From the Nyquist plots, it can be seen that as compression increases, the radius of the capacitive loops keeps decreasing, suggesting that during corrosion, as dislocation density increases, the corrosion resistance of high-purity magnesium decreases, and the resistance of the formed corrosion product diminishes. This implies a certain positive correlation between dislocation density in high-purity magnesium and corrosion rate.

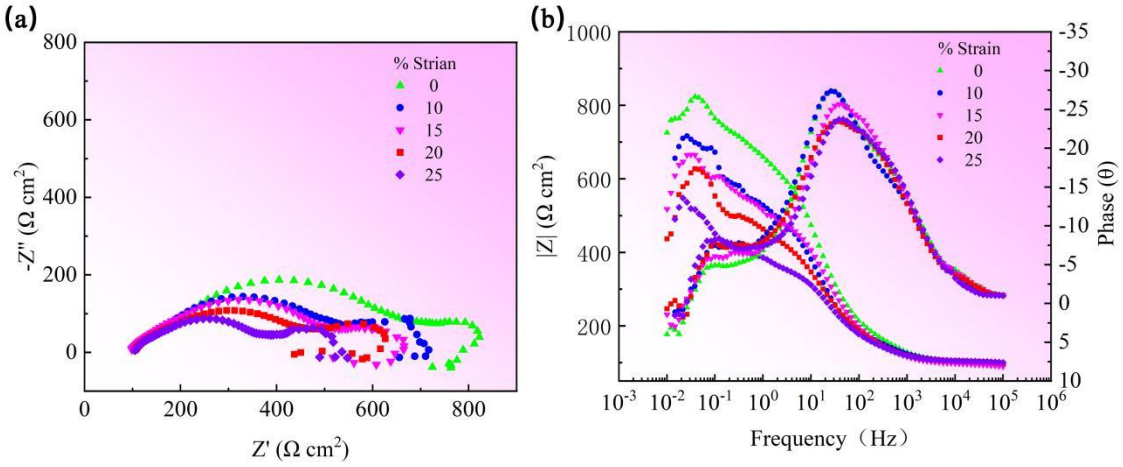


Figure 8 EIS spectra of samples with different compressive strains in m-SBF solution: (a) Nyquist plot; (b) Bode plot

To further study the corrosion differences of these compressed strain-treated samples, as shown in **Figure 9**, researchers quantitatively analyzed the EIS spectra by fitting equivalent circuits.

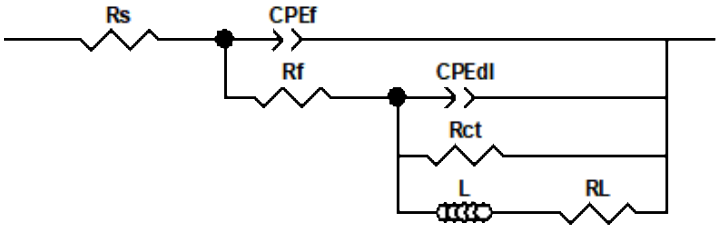


Figure 9 EIS fitting circuit

The detailed data of the fitting circuits are shown in **Table 2**. Here, Rs represents the solution resistance, while Rf and CPEf represent the resistance and capacitance of the corrosion product film, reflecting the first capacitive

loop in the high-frequency region. The constant phase element (CPE) is used to compensate for non-uniformities in the system; it represents the capacitive effects associated with non-ideal capacitor behavior. The impedance of the CPE is related to frequency as follows:

$$Z_{CPE} = 1 / T(i\omega)^n \quad (5)$$

where T is the magnitude of the CPE and n is its exponent [19]. The parallel-connected Rdl and CPEdl represent the charge transfer resistance and double-layer capacitance, respectively. This corresponds to the parameters describing the second capacitive loop. Generally, the higher the value of Rf, the better the protective effect of the corrosion product film, and the larger the Rct, the lower the corrosion rate of high-purity magnesium. The fitting results obtained using Z-View2 software are summarized in **Table 2**, and the fitting curves are displayed as solid lines in Figure 8. Based on the fitting results, the 25% Rct value is the lowest at 116.52 $\Omega \cdot cm^2$, indicating that a higher dislocation density leads to a faster corrosion rate. The values of the corrosion film resistance Rf related to the corrosion products formed on the surfaces of samples with different dislocation densities are as follows: 0% Strain (625.11 $\Omega \cdot cm^2$) > 10% Strain (453.86 $\Omega \cdot cm^2$) > 15% Strain (449.90 $\Omega \cdot cm^2$) > 20% Strain (414.86 $\Omega \cdot cm^2$) > 25% Strain (311.14 $\Omega \cdot cm^2$), showing that corrosion products on samples with low dislocation density provide better protection.

Table 2 Fitted circuit data table based on EIS

Strain	0%	10%	15%	20%	25%
Rs（$\Omega \cdot cm^2$）	105.63	104.87	104.23	103.61	101.98
CPEf-T（$\times 10^{-5} \Omega^{-1} \cdot cm^{-2} \cdot s^n$）	2.82	3.10	2.65	5.00	4.52
CPEf-n	0.6502	0.6927	0.6681	0.5973	0.6282
Rf（$\Omega \cdot cm^2$）	625.11	453.86	449.90	414.86	311.14
CPEdl-T（$\Omega^{-1} \cdot cm^{-2} \cdot s^n$）	0.0068	0.0024	0.0037	0.0058	0.0046
CPEdl-n	0.8306	0.9512	0.9022	0.9249	0.9603
Rct（$\Omega \cdot cm^2$）	257.73	156.48	132.34	122.96	116.52
L($H \cdot cm^2$)	462.90	512.34	543.88	563.22	621.82
RL（$\Omega \cdot cm^2$）	34.76	36.19	37.95	42.17	45.92
χ^2	5.2×10^{-3}	4.2×10^{-3}	4.8×10^{-3}	4.6×10^{-3}	4.3×10^{-3}

To take a closer look at how dislocation density affects the corrosion rate of high-purity magnesium, we used SEM to observe the morphology after electrochemical corrosion. As shown in **Figure 10**, the surface of high-purity magnesium developed a continuous layer of corrosion products, along with typical drying shrinkage cracks；From the EDS map (see supplementary material 1), you can see that Mg, O, Ca, and P are evenly distributed on the surface.

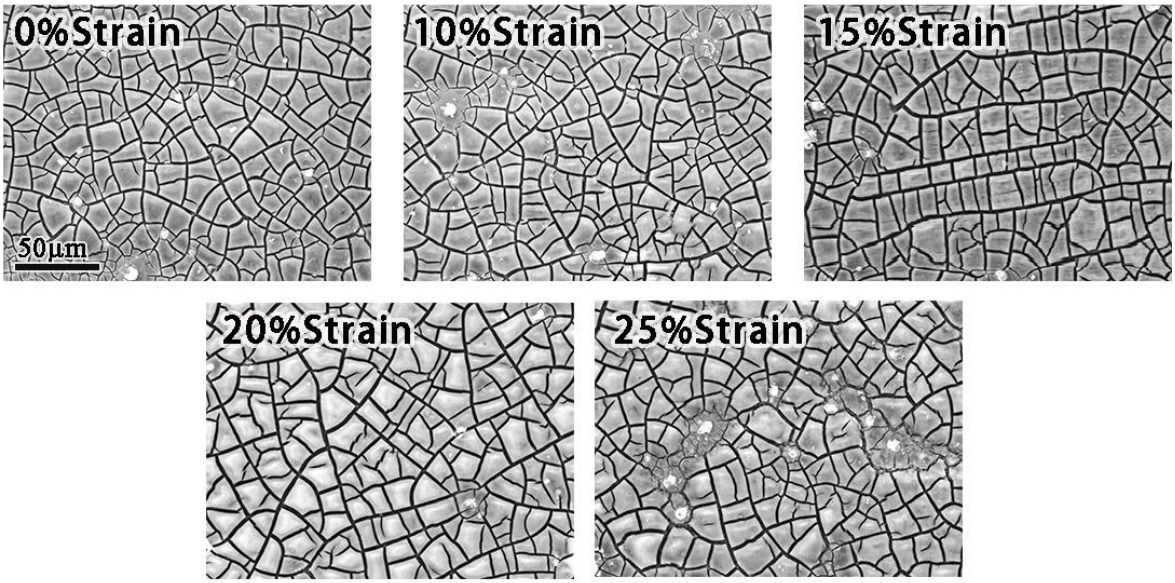


Figure 10 Electrochemical corrosion morphology of high-purity magnesium under different compressive strains

3.2. Test Results of Different t-HPS Turns Groups

3.2.1. Microstructure Testing of Different t-HPS Turns

The microstructure of high-purity magnesium under different t-HPS turns can be seen in **Figure 11**: 10 Turns (Figure (a1)), 15 Turns (Figure (b1)), 20 Turns (Figure (c1)), and 25 Turns (Figure (d1)).

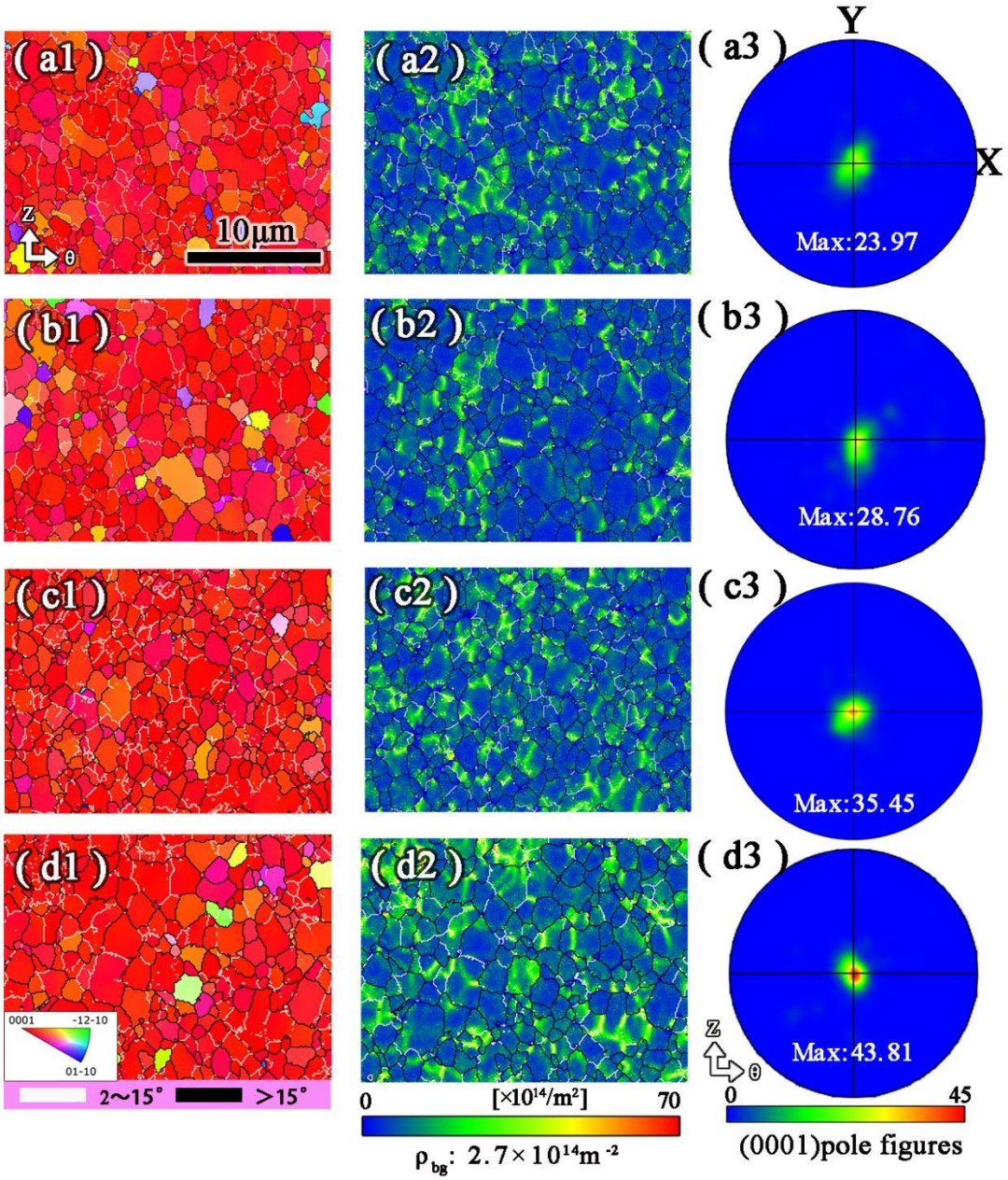


Figure 11 EBSD maps for different numbers of turns: 10Turn, 15Turn, 20Turn, 25Turn; microstructure images (a1–d1); geometrically necessary dislocation maps (a2–d2); (0001) pole figures (a3–d3)

From Figures a1 to d1, we can see that the grain orientations of the samples remain consistent, and the grain sizes are very similar. Detailed analysis, as shown in **Figure 12**, indicates that the average grain size is from *1.28 to 1.35* μm. Within the margin of error, we can say that the grain size of the samples does not change during t-HPS process, so we can rule out any effect of grain size on the corrosion performance in this set of samples.

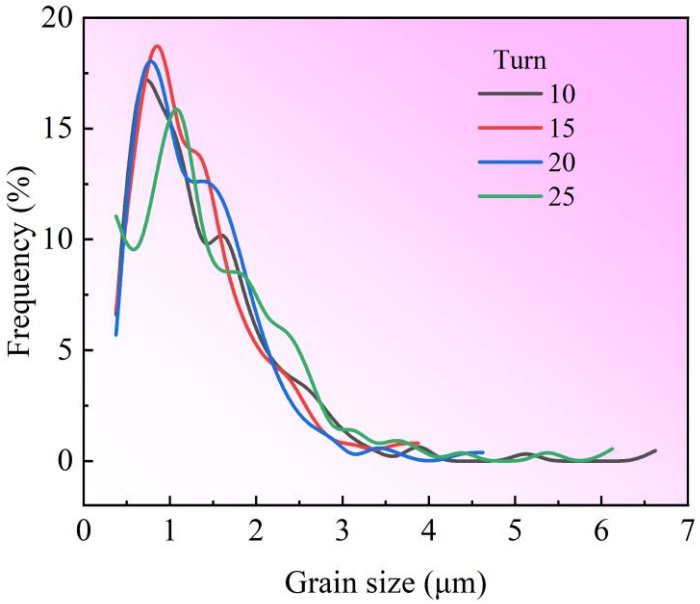


Figure 12 Equivalent circular diameter distribution of t-HPS high-purity magnesium samples with different turns

The dislocation densities are $9.12\pm0.13\times10^{14}/m^2$, $8.4\pm0.16\times10^{14}/m^2$, $10.14\pm0.20\times10^{14}/m^2$, and $12.18\pm0.17\times10^{14}/m^{22}$. The textures of these four samples, shown in Figure 12(a3)~(d3), are very similar, with grains mainly oriented along (0001). The maximum texture intensity of the 10-turn to 25-turn samples are 23.97, 28.76, 35.45, and 43.81, respectively, indicating that the texture intensity of this group of four samples keeps increasing with the number of turns.

3.2.2. Corrosion Test

To explore how the corrosion rate of t-HPS samples with different numbers of turns changes in m-SBF, we conducted a 168-hour immersion test. The test results are shown in **Figure 13**, and the sample with 20 turns had the slowest corrosion rate.

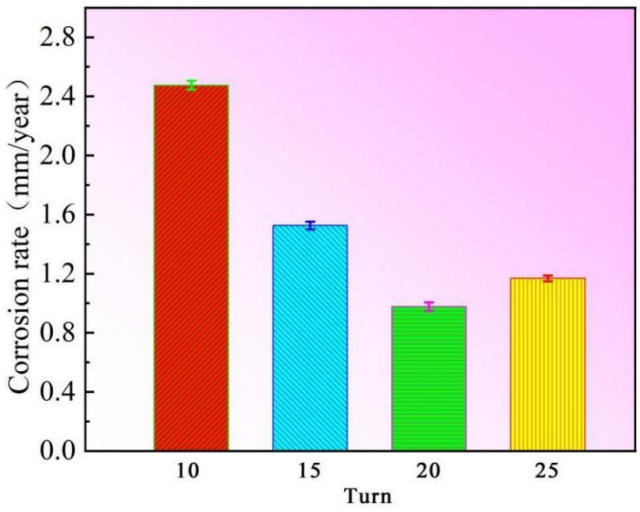


Figure 13 Corrosion rates after 168h m-SBF immersion tests with different t-HPS turns

Figure 14 shows the corrosion morphology of high-purity magnesium after being immersed in m-SBF for 168 hours. It's clear that the 10Turn sample has the most severe corrosion, with obvious grain boundary corrosion features, some aggregation of corrosion products, and tiny corrosion pits, showing a mix of localized and uniform corrosion. The 15Turn sample has a more continuous and dense layer of corrosion products on the surface, with reduced cracks and grooves, making the corrosion more uniform. Both the 20Turn and 25Turn samples exhibit clearly uniform corrosion.

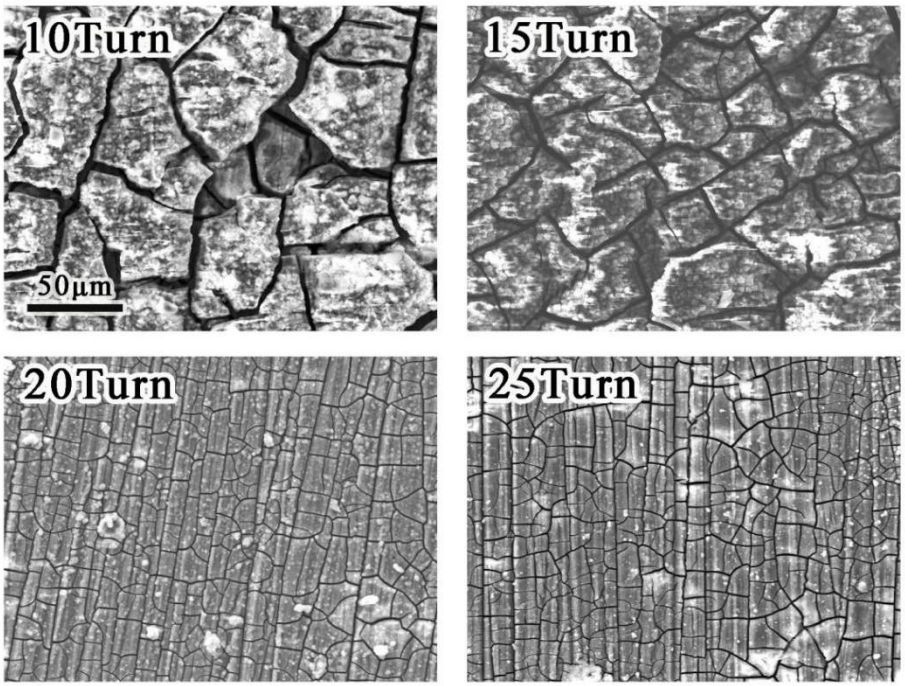


Figure 14 SEM schematic of t-HPS samples with different turns after 168 hours of immersion in SBF

Figure 15 shows the SEM images after cleaning. The sample with 10 turns developed deeper corrosion pits, while the 20-cycle sample showed more uniform corrosion with shallower pits.

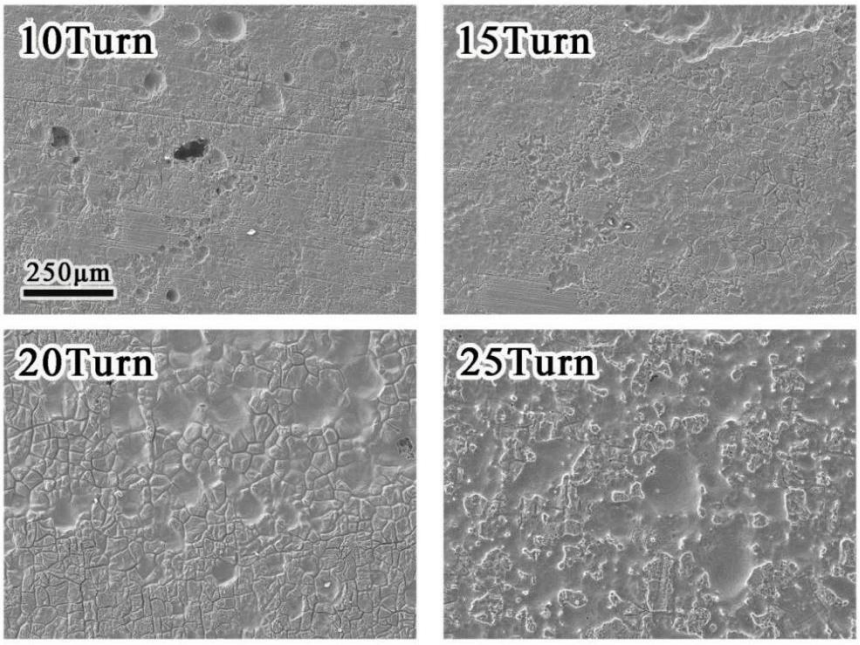


Figure 15 SEM schematic of t-HPS samples with different turns after 168h immersion in SBF and cleaning

Through electrochemical polarization tests and electrochemical impedance tests, we can preliminarily assess how the dislocation density and texture intensity of samples with different turns affect the corrosion behavior of high-purity magnesium in m-SBF. As shown in **Figure 16**, under the influence of dislocation density and texture intensity, the higher the dislocation density, the faster the corrosion rate, which aligns with the findings from the compression strain group. Additionally, it's evident that texture intensity positively impacts the corrosion resistance of high-purity magnesium, slowing down the corrosion rate of the samples. The specific corrosion potential and corrosion current density are listed in **Table 3**.

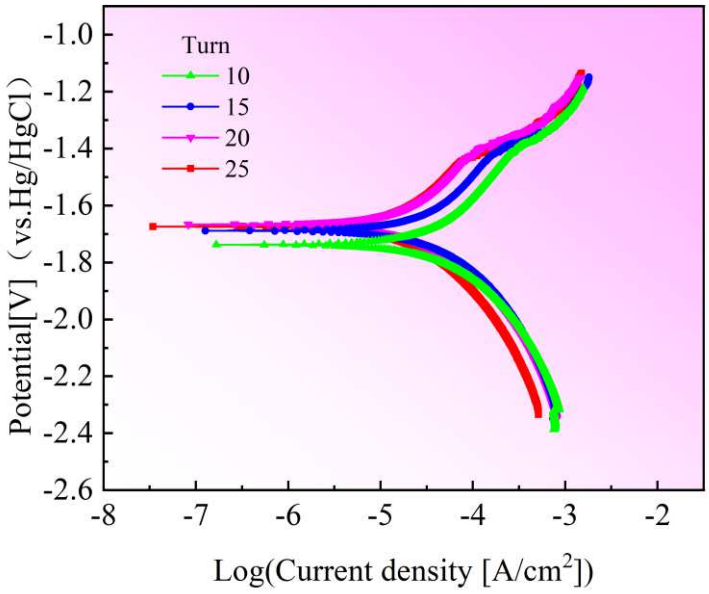


Figure 16 Electrochemical polarization curves of high-purity magnesium in m-SBF solution at different t-HPS turns

Table 3 Corrosion voltage and current values of t-HPS samples with different turns in m-SBF solution

Turn	Ecorr（V vs.Hg/HgCl）	Icorr（A/cm^2）
10	-1.74±0.04	2.07±0.12×10^{-5}
15	-1.69±0.02	1.71±0.16×10^{-5}
20	-1.66±0.05	9.01±0.12×10^{-6}
25	-1.67±0.06	9.96±0.15×10^{-6}

Figure 17 shows the EIS spectra of these samples after soaking in m-SBF solution for 1 hour. All four sets of samples have two capacitive loops and one inductive loop, which can also be fitted using the equivalent circuit in **Figure 9**. From the Nyquist plot in Figure 17(a), we can see that $CR_{20Turn} < CR_{25Turn} < CR_{15Turn} < CR_{10Turn}$. The fitted current data is shown in Table 4, from which we can see that the 20-turn sample has the highest Rf and Rct, indicating that the surface corrosion resistance of high-purity magnesium is best at 20 turns.

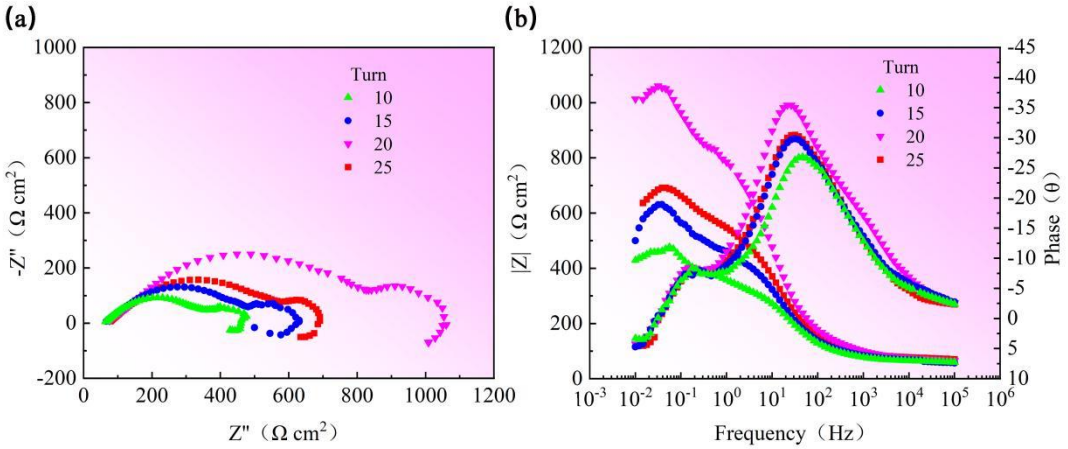


Figure 17 EIS spectra of t-HPS samples with different turns counts in m-SBF solution: (a) Nyquist plot; (b) Bode plot

Table 4 Fitted circuit data table based on EIS

	10Turn	15Turn	20Turn	25Turn
Rs（$\Omega \cdot cm^2$）	63.16	66.38	80.15	79.58
CPEf-T（$\times 10^{-5} \Omega^{-1} \cdot cm^{-2} \cdot s^n$）	4.56	4.79	2.63	3.11
CPEf-n	0.6477	0.6302	0.6850	0.6922
Rf（$\Omega \cdot cm^2$）	320.47	459.79	804.28	508.40
CPEdl-T（$\Omega^{-1} \cdot cm^{-2} \cdot s^n$）	0.0036	0.0047	0.0023	0.0027
CPEdl-n	0.8713	0.8412	0.9515	0.9524
Rct（$\Omega \cdot cm^2$）	104.22	110.88	186.57	115.78
L($H \cdot cm^2$)	1133.51	817.56	612.4	766.21
RL（$\Omega \cdot cm^2$）	47.56	49.31	58.12	53.76
χ^2	4.5×10^{-3}	4.9×10^{-3}	4.7×10^{-3}	5.1×10^{-3}

Similar to the compressed strain group, these four groups of samples were also examined using SEM to observe their electrochemical corrosion morphology. The results are shown in **Figure 18**, showing a dense corrosion product film and cracks caused by residual stress.

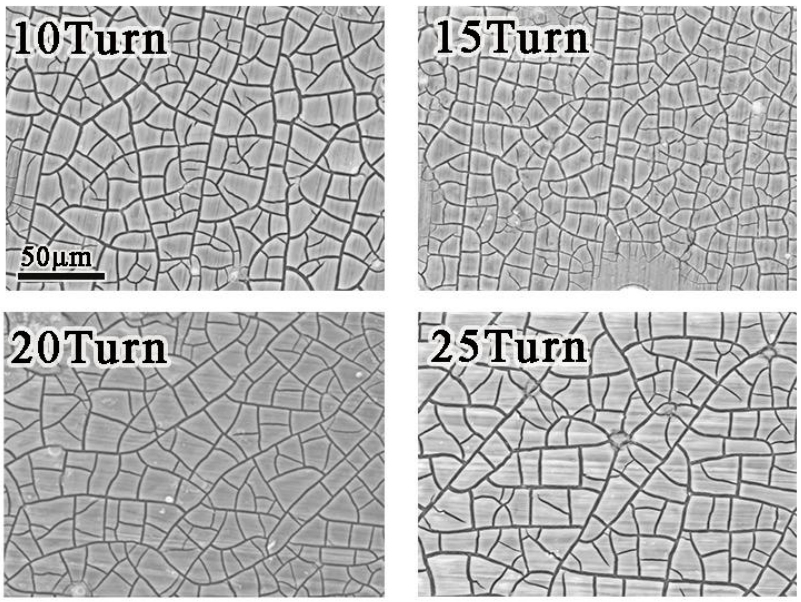


Figure 18 Electrochemical corrosion morphology images of high-purity magnesium at different t-HPS turns

4. Discussion

From the samples in the compressed strain group, we can see that the grain size and texture intensity of the samples basically remain unchanged, and only the dislocation density increases with the increase of compressive strain. Therefore, we can just discuss the effect of dislocation density on the corrosion rate of high-purity magnesium. Based on the experimental results, we plotted the relationship between dislocation density and the corrosion rate of high-purity magnesium (**Figure 19**), and then used Origin software to fit a correlation formula as follows:

$$CR=0.0302*(\rho-6.6213)^2+0.6437 \quad (6)$$

Here, CR represents the corrosion rate of high-purity magnesium in SBF immersion tests, indicating dislocation density, with $\rho > 6.62$ ($\times 10^{14}/m^2$).

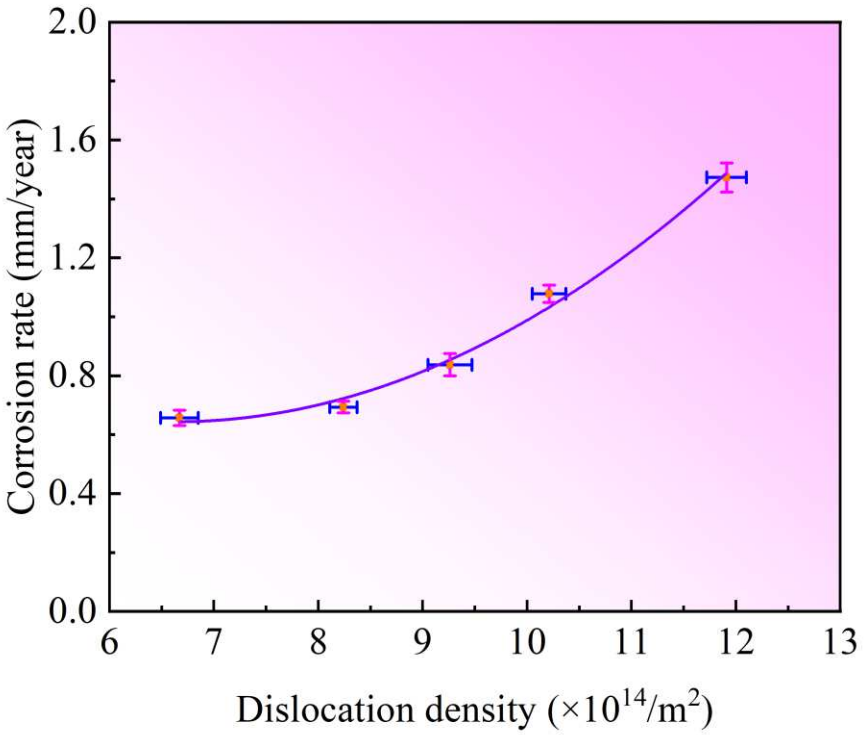


Figure 19 Graph of dislocation density and corrosion rate of high-purity magnesium in m-SBF

From the figure, it can be seen that as the dislocation density increases, the corrosion rate shows a clear upward trend, and the fitted curve appears as an upward-convex quadratic growth relationship. This indicates that dislocation density promotes corrosion, and this promoting effect is more significant in regions with high dislocation density. This is because dislocation areas are active sites for corrosion; the denser the dislocations, the more active sites there are, and the faster the corrosion rate. In addition, as Bahmani A and others noted [25], dislocations can act as anodic points compared to the matrix, accelerating corrosion. Therefore, the higher the dislocation density, the faster the corrosion rate.

Through t-HPS at 150°C with different numbers of turns, we obtained high-purity magnesium samples with varying texture intensitys and dislocation densities while keeping the grain size roughly the same. After different corrosion tests, we found that $CR_{10Turn} > CR_{15Turn} > CR_{25Turn} > CR_{20Turn}$. Combining this with the fitted results from the compression strain group, it's easy to establish a phenomenological model linking dislocation density, texture intensity, and the corrosion rate of high-purity magnesium(**Figure 20**). From this, an empirical formula was also derived:

$$CR=0.03016\rho^2-0.3994\rho+1704.5T^{-2}+0.6396 \quad (7)$$

Here, CR represents the corrosion rate of high-purity magnesium in m-SBF, T represents the texture intensity of the sample, and ρ represents the dislocation density of the sample. Need to meet the following relationship：

$$T > 50.75,\ \rho > \frac{0.6456 + \sqrt{0.1170 - \frac{301.3}{T^2}}}{0.08578} \quad (8)$$

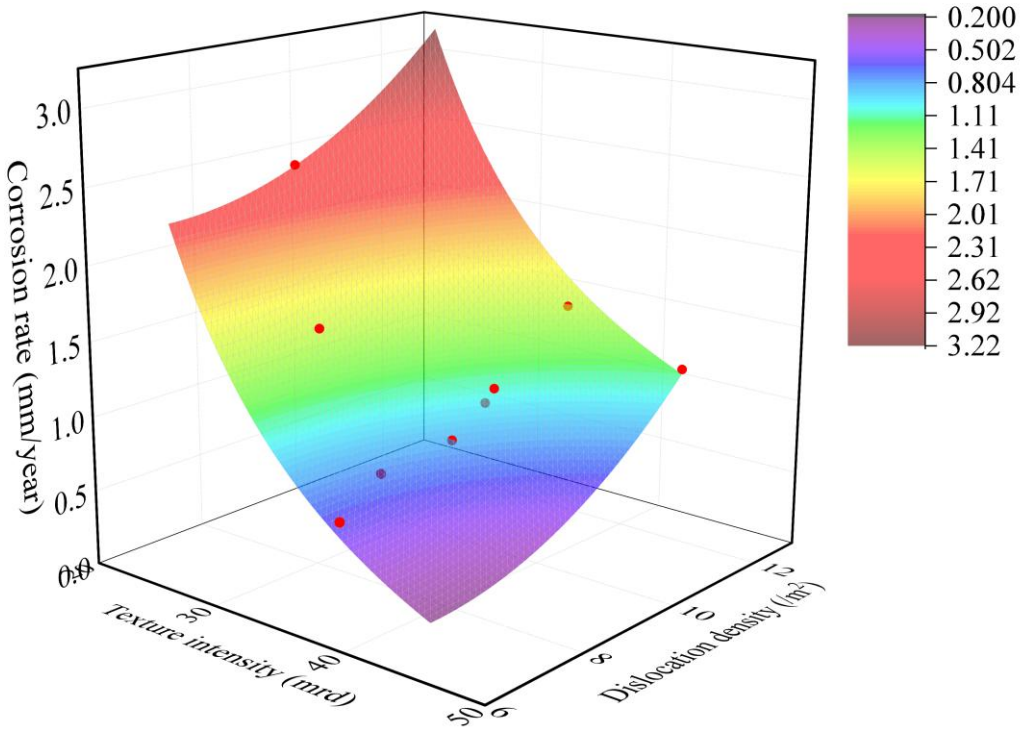


Figure 20 Phenomenological model of dislocation density, texture intensity, and the corrosion rate of high-purity magnesium in m-SBF

Based on the obtained phenomenological model, it's easy to figure out that the relationship between texture intensity and corrosion rate is as follows:

$$CR \propto T^{-2} \quad (9)$$

Under the condition that other factors remain unchanged, as the texture intensity of the basal plane increases, the corrosion rate of high-purity magnesium in m-SBF keeps decreasing, and the rate of decrease gradually slows down. We think this is because the (0001) plane has the highest atomic density and the lowest surface energy[26], making it more corrosion-resistant compared to other crystal planes. Additionally, when different crystal planes coexist on the surface, galvanic corrosion can occur between the basal plane and other planes[27]. As the texture intensity increases, the proportion of the (0001) planes goes up, which reduces galvanic corrosion and slows down the corrosion rate. However, as the texture intensity continues to increase and most of the surface becomes (0001) planes, the effect of texture intensity weakens, which is shown by the curve becoming less steep.

5. Conclusion

This study adopts compression and t-HPS experimental designs in an attempt to separate the effects of grain size and dislocation density, thereby isolating texture intensity. Through microstructural testing, electrochemical analysis, and immersion experiments, a quantitative relationship between isolated texture intensity and the corrosion rate of high-purity magnesium is ultimately obtained. The main research conclusions are as follows:

(1) By applying compression without changing grain size and texture intensity, only the dislocation density is altered. An increase in dislocation density raises the crystal's energy, increases the active corrosion sites in high-purity magnesium, and consequently leads to a higher corrosion rate in m-SBF.

(2) By increasing the number of t-HPS passes, the actual strain is increased. Running at 150°C, the grains simultaneously undergo recrystallization and refinement, and their mutual interaction keeps the grain size largely unchanged.

(3) The effect of texture and dislocation density on corrosion property are independent, and thus additive.

(4) Combining the results from samples with different numbers of passes and the dislocation density data from different compressive strain groups, the relationship between texture intensity and corrosion rate was ultimately obtained as follows:

$$CR=1704.5T^{-2}+b$$

Here, CR stands for the corrosion rate of high-purity magnesium in m-SBF, and T represents the texture intensity of the sample, b is a constant.

References

[1] Chen Y, Zhang S, Bai J, et al. Magnesium-based biomaterials for coordinated tissue repair: A comprehensive overview of design strategies, advantages, and challenges[J]. Journal of Magnesium and Alloys, 2024, 12(8): 3025-3061.

[2] Chen Y , Xu Z , Smith C ,et al.Recent advances on the development of magnesium alloys for biodegradable implants[J].Acta Biomaterialia, 2014, 10(11):4561-4573.

[3] Han H S, Loffredo S, Jun I, et al. Current status and outlook on the clinical translation of biodegradable metals[J]. Materials Today, 2019, 23: 57-71.

[4] Kraus T , Fischerauer S F ,Anja C Hänzi,et al.Magnesium alloys for temporary implants in osteosynthesis: In vivo studies of their degradation and interaction with bone[J].Acta Biomaterialia, 2012, 8(3):1230-1238.

[5] Han P , Cheng P , Zhang S ,et al.In vitro and in vivo studies on the degradation of high-purity Mg (99.99wt.%) screw with femoral intracondylar fractured rabbit model[J].Biomaterials, 2015, 64:57-69.

[6] Ralston K D , Birbilis N , Davies C H J .Revealing the relationship between grain size and corrosion rate of metals[J].Scripta Materialia, 2010, 63(12):1201-1204.

[7] Song D , Ma A B , Jiang J ,et al.Corrosion behavior of equal-channel-angular-pressed pure magnesium in NaCl aqueous solution[J].Corrosion Science, 2010, 52(2):481-490.

[8] Song G L , Xu Z .Crystal orientation and electrochemical corrosion of polycrystalline Mg[J].Corrosion Science, 2012, 63(OCT.):100-112.

[9] Shin K S , Bian M Z , Nam N D .Effects of Crystallographic Orientation on Corrosion Behavior of Magnesium Single Crystals[J].JOM, 2012, 64(6):p.664-670.

[10] Wang B J , Xu D K , Dong J H ,et al.Effect of the crystallographic orientation and twinning on the corrosion resistance of an as-extruded Mg–3Al–1Zn (wt.%) bar[J].Scripta Materialia, 2014, 88(2):5-8.

[11] Han G , Lee J Y , Kim Y C ,et al.Preferred crystallographic pitting corrosion of pure magnesium in Hanks' solution[J].Corrosion Science, 2012, 63(OCT.):316-322.

[12] Bahmani A , Arthanari S , Shin K S .Formulation of corrosion rate of magnesium alloys using microstructural parameters[J].Journal of Magnesium and Alloys, 2020, 8(1).

[13] Wang X, Chen C, Li L, et al. Microstructure design for biodegradable magnesium alloys based on biocorrosion behavior by macroscopic and quasi-in-situ EBSD observations[J]. Corrosion Science, 2023, 221: 111366.

[14] Bai J, Sun C, Wang C, et al. Gradient textures induce micro-galvanic corrosion on Mg[J]. Journal of Alloys and Compounds, 2024, 1005: 176119.

[15] Li Z, Liu Y, Wang J T, et al. Tube high-pressure shearing: a simple shear path to unusual microstructures and unprecedented properties[J]. Materials Transactions, 2023, 64(7): 1449-1463.

[16] Wang J T , Li Z , Wang J ,et al.Principles of severe plastic deformation using tube high-pressure shearing[J].Scripta Materialia, 2012, 67(10):810–813.

[17] Standard A. Standard practice for laboratory immersion corrosion testing of metals[J]. American Society for Testing and Materials G31-72, 2004.

[18] American Society for Testing and Materials (Filadelfia, Pa.). ASTM G1-03: Standard Practice for Preparing, Cleaning, and Evaluating Corrosion Test Specimens[C]. ASTM, 2004.

[19] Wang C , Sun M , Yang C ,et al.Degradation behavior of pure Mg in the physiological medium and growth mechanism of surface corrosion product films[J].Journal of Magnesium and Alloys, 2025, 13(4):1523-1535.

[20] Frankel G S , Samaniego A , Birbilis N .Evolution of hydrogen at dissolving magnesium surfaces[J].Corrosion Science, 2013, 70(3):104-111.

[21] Triviño-Peláez Á, Reyes-Riverol R, Fajardo S. On the interfacial kinetic origin of the mid-and low-frequency impedance response during magnesium corrosion[J]. Electrochimica Acta, 2026: 148641.

[22] Bonora P L , Andrei M , Eliezer A .Corrosion behaviour of stressed magnesium alloys[J].Corrosion Science, 2002, 44(4):729-749.

[23] Wang W , Wu H , Sun Y ,et al.Local intragranular misorientation accelerates corrosion in biodegradable Mg[J].Acta biomaterialia, 2020, 101:575-585.

[24] Gomes M P , Costa I ,Nadine Pébère,et al.On the corrosion mechanism of Mg investigated by electrochemical impedance spectroscopy[J].Electrochimica Acta, 2019, 306(000):10.

[25] Bahmani A , Lotfpour M , Taghizadeh M ,et al.Corrosion behavior of severely plastically deformed Mg and Mg alloys[J].Journal of Magnesium and Alloys, 2022, 10(10):2607-2648.

[26] Liu M , Qiu D , Zhao M C ,et al.The effect of crystallographic orientation on the active corrosion of pure magnesium[J].Scripta Materialia, 2008, 58(5):421-424.

[27] Gerashi E , Alizadeh R , Langdon T G .Effect of crystallographic texture and twinning on the corrosion behavior of Mg alloys:A review[J].Journal of Magnesium and Alloys, 2022, 10(2):332-345.

Supplementary Files

This is a list of supplementary files associated with this preprint. Click to download.

- SupplementaryMaterial1.docx